Journal Pre-proof

Magnetic Field Platform for Well-Mixed and Spatially-Structured Experiments on Microbial Populations

Akila Bandara, Enoki Li, Daniel A. Charlebois

PII: S2667-0747(24)00024-7

DOI: https://doi.org/10.1016/j.bpr.2024.100165

Reference: BPR 100165

To appear in: *Biophysical Reports*

Received Date: 18 January 2024

Revised Date: 31 May 2024

Accepted Date: 13 June 2024

Please cite this article as: Bandara A, Li E, Charlebois DA, Magnetic Field Platform for Well-Mixed and Spatially-Structured Experiments on Microbial Populations, *Biophysical Reports* (2024), doi: https://doi.org/10.1016/j.bpr.2024.100165.

Magnetic Field Platform for Well-Mixed and Spatially-Structured Experiments on Microbial Populations

Akila Bandara[1], Enoki Li[1], and Daniel A. Charlebois[1,2]

[1]Department of Physics, University of Alberta, Edmonton, Alberta, T6G-2E1, Canada
[2]Department of Biomedical Engineering, University of Alberta, Edmonton, Alberta, T6G-1H9, Canada

E-mail: dcharleb@ualberta.ca

Abstract.

Magnetic fields have been shown to affect sensing, migration, and navigation in living organisms. However, the effects of magnetic fields on microorganisms largely remain to be elucidated. We develop an open-source, 3D-printed magnetic field exposure device to perform experiments on well-mixed and spatially-structured microbial populations. This device is designed in AutoCAD, modeled in COMSOL, and validated using a Gaussmeter and experiments on the budding yeast *Saccharomyces cerevisiae*. We find that static magnetic field exposure slows the spatially-structured expansion of yeast mats that expands in two dimensions, but not yeast mats that expand in three dimensions, across the surface of semi-solid yeast extract-peptone-dextrose (YPD) agar media. We also find that magnetic fields do not affect the growth of planktonic yeast cells in well-mixed liquid YPD media. This study provides an adaptable device for performing controlled magnetic field experiments on microbes and advances our understanding of the effects of magnetic fields on fungi.

Keywords: fungal mats, magnetic field device, microbial population experiments, planktonic fungi, *Saccharomyces cerevisiae*

Why It Matters?

Microorganisms have been shown to be affected by magnetic fields. However, the effects of magnetic phenomena on microbial populations are largely unknown. This is especially true for fungi, which are important microorganisms for microbiological research, industrial applications, and infectious disease. To study magnetobiological phenomena, we need devices to perform controlled experiments in a variety of conditions. We develop an open source, 3D-printed magnetic field platform using computer-aided design and physics modeling software to study the effects of magnetic fields on microbial populations. Using this magnetic field device, we find that magnetic fields can slow the growth of budding yeast on agar plates, but that magnetic fields do not affect the growth of budding yeast in liquid media.

1. Introduction

The effect of electromagnetic fields (EMFs) on the adaptation and evolution of life on Earth is an ongoing area of research [1]. Living organisms including sharks, bees, and birds use

EMFs to sense, navigate, and migrate [2]. Magnetic fields (MFs) have been shown to affect the germination of plants [3], the orientation of blood cells [4, 5], and alter stem cell mediated growth of flatworms [6]. Magnetotactic bacteria can align with external MFs by biomineralizing magnetic nanoparticles (magnetite or greigite) inside organelles called magnetosomes, which is thought to aid bacteria to reach regions of optimal oxygen concentration [7]. Magnetic nanoparticles have been implemented in cell labeling and imaging [8], as well as targeted drug delivery applications [9]. Despite the advantages of EMFs for living microorganisms, it is important to investigate the detrimental effects of EMF exposure [10].

Due to a short replication time, ease of culture, and well-characterized eukaryotic genetic background, the budding yeast *Saccharomyces cerevisiae* is a ubiquitous model organism in molecular biology [11]. *S. cerevisiae* has been used as a model organism in EMF and MF exposure studies [12, 13, 14, 15, 16, 17]. For instance, using a single-cell MF device the orientation of individual *S. cerevisiae* cells was found to align with a static MF during budding [12]. Exposure to a strong 50000 G vertical MF resulted in changes in the sedimentation pattern of yeast cells depending on their location in the culture dishes [14]. However, in the same study, no changes in gene expression were observed after exposure to a 50,000 G MF (for 2 and 24 hours) or to a 100,000 G MF (for 1 hour).

Previous studies highlight the necessity to study the isolated effects of MFs on fungi. For example, exposing plant pathogenic fungi to low-frequency EMFs and MFs separately yields diverging results: EMFs (1 G at 50 Hz) were found to have no effect on the growth of mycorrhizal fungi [18], whereas MFs ($1 - 10$ G) slowed the growth of phytopathogenic fungi [17]. Another study found that exposing non-pathogenic *S. cerevisiae* cells to stronger EMFs (50 Hz with inductions up to 10 mT, with exposure times up to 24 minutes) decreased the viability of yeasts cells and slowed their growth [19]. More recently, a 2D lattice-based Monte Carlo simulation framework was developed to investigate the effects of nutrient concentration and MF exposure on yeast colony growth and morphology [20]. Simulation of this framework predicted that prolonged MF exposure will decrease colony growth and alter colony morphology. Despite this research, our knowledge of the effects of MFs on fungi remains limited [17]. Furthermore, though there are many studies on organisms exposed to EMFs (e.g., [19, 21, 22, 23, 24]), the effects of static MF on the growth and development of microorganisms largely remain to be investigated [12].

Yeast exist as part of microbial communities, including colonies, biofilms [25] and "mats" [26, 27, 28, 29, 30]. A yeast mat is a morphologically complex, colony-like structure that requires the expression of the flocculin gene *flo11*, which encodes the *Flo11* surface adhesion protein. Chen *et al.* [31] cultured strains of genetically engineered *S. cerevisiae* cells with and without the *flo11* gene, respectively called TBR1 and TBR5. "Wild-type" TBR1 mats (formed from TBR1 cells with a functional copy of *flo11*) displayed a rough surface, pattern forming phenotype, whereas mutant TBR5 mats (formed from cells lacking a functional copy of *flo11*) displayed a smooth surface phenotype. TBR1 mats grew faster and larger compared to TBR5 mats on semi-solid agar plates; TBR1 also outcompeted TBR5 in competition assays. TBR1 mats are constrained to expand in 2D along the agar surface due to the expression of *Flo11* in TBR1 cells. As a result, TBR1 mats had a higher growth rate (fitness) than TBR5 mats, which expand in three dimensions, resulting in a slower

mat expansion rate and size along the agar surface. In contrast, there was no difference in fitness between TBR1 and TBR5 strains in liquid culture experiments [31]. Other studies have found similar results for TBR1 and TBR5 growth rates in semi-solid and liquid media cultures [26, 32]. Given the discernible phenotypes and differential growth rates of the TBR1 and TBR5 strains on agar media, this model system is ideal to investigate the effects of MF exposure on population growth dynamics and to generate hypotheses on the underlying biophysical mechanisms.

In this study, we develop an adaptable, open-source MF exposure platform to investigate of the affects of MF on microbial population over extended periods. The device consists of two Neodymium ($Nd_2Fe_{14}B$) magnets that expose multiple biological replicates to a static MF in the range of 350 G to 1500 G. The compact design of the MF device allows it to be placed inside of an incubator or environmental chamber to perform controlled experiments. We design the MF exposure device in AutoCAD [33] and optimize the design via numerical simulations in COMSOL Multiphysics [34]. We then 3D print the optimized device and measure the MF inside the sample exposure region, which is compared to numerical COMSOL simulations. To highlight the utility of our device, we perform MF experiments on well-mixed and spatially-structured yeast populations inside of an environmental chamber. We find that 1) horizontal and vertical MFs slow the growth of TBR1 mats on semi-solid agar media, but that MFs do not affect the growth of TBR5 mats; 2) TBR1 and TBR5 mats adapt over the duration of the experiment to increase their growth rates on agar media in both the presence and absence of MFs; and 3) MFs do not affect the growth rate of planktonic TBR1 and TBR5 cells in liquid media.

2. Materials and Methods

2.1. Fabricating the MF exposure device

Previous experiments established that a range of magnetic flux densities ($\vec{B}$) affect the growth or the orientation of yeast cells, ranging from 100 G [19] to 29300 G [12]. Motivated by these studies, we developed an adaptable, open-source platform capable of generating horizontal or vertical homogeneous MFs within this range. This MF device was designed to perform controlled and repeatable long-term, population-scale magnetobiological experiments on microorganisms. As such, the MF device was optimized to be placed in an incubator/environment chamber, while having the capacity to accommodate multiple biological replicates of microbes cultured in standard-size culture tubes and Petri dishes. The AutoCAD, COMSOL, and 3D printing files are freely available online (see Supporting Materials) to facilitate the replication and adaptation of our platform by other research groups for their magnetobiological experiments.

To create a homogeneous MF to expose biological samples of microbes growing in cell culture tubes or Petri dishes, we used two N52 grade $Nd_2Fe_{14}B$ block magnets (Amazing Magnets Inc, Catalog no. Q500Y-N52). The device's ability to hold multiple replicates (five Petri dishes or nineteen culture tubes) for each exposure experiment is essential to ensure the repeatability of the results and to test for statistical significance. The horizontal and vertical configurations of the block magnets in the device permit MF exposure emanating from two different directions (Figs. 1A,B and C1). With dimensions of $101.6 \times 101.6 \times 12.7\ mm^3$, these

magnets were capable of producing a $\vec{B}$ of approximately 14400 G at the magnets surface, which is five orders of magnitude stronger than the Earth's MF (0.24 G to 0.66 G depending on the latitude [35]).

The MF exposure device materials were selected to minimize interaction between the magnets and the scaffolding. Considering that microorganisms will typically be grown on semi-solid media in Petri dishes or in liquid media in culture tubes (see Section 2.3), it was necessary to fabricate the MF device using a material that had compatible magnetic permeability (μ) to the Petri dishes and culture tubes. This ensures that the homogeneous MFs produced by the block magnets would have the least possible interference during its path towards the exposure samples [36]. Since two strong magnets are in close proximity (132 mm), the device materials need to be sufficiently strong to withstand a pull force of 5.78 N without compromising the structural integrity of the device. Furthermore, as the device is intended to perform experiments on biological samples, it was designed to be disassembled so that the components can be cleaned and sterilized.

A cross sectional area of 101.6 $\times$ 101.6 mm^2 ensured that the magnets generated a homogeneous MF throughout the sample exposure region. While the magnitude of MF strength varied spatially throughout the exposure region, the direction of the field is almost uniform (Figs. 2A and 3A), and, therefore no "edge effects" were introduced in our MF exposure experiments. This assured that the yeast colonies grown in both liquid and semi-solid media were exposed only to homogeneous MF, thus avoiding MF edge effects.

We used AutoCAD [33] to design a MF device with two interchangeable configurations: a horizontal $\vec{B}$ configuration and a vertical $\vec{B}$ configuration (see Fig. C1). COMSOL Multiphysics [34] was used to simulate the MF inside the device to optimize the design (see Section 3.1). The "Magnetic Fields, No currents" interface in the AC/DC module of COMSOL was used to simulate the $\vec{B}$ values within exposure region of the MF device via a finite element method [37]. The MF strength ($\vec{H}$) and the $\vec{B}$ resulting from the permanent magnets in the exposure device are respectively described by Maxwell's equations for a static MF [38]:

$$\nabla \times \vec{H} = 0 \tag{1}$$

and

$$\nabla \cdot \vec{B} = 0. \tag{2}$$

From Equation (1), we can define the magnetic scalar potential (V_m) as:

$$\vec{H} = -\nabla V_m, \tag{3}$$

and considering the relation between the $\vec{B}$ and $\vec{H}$ yields:

$$\vec{B} = \mu_0 \mu_{rec} \vec{H} + \vec{B}_r, \tag{4}$$

where μ_0, μ_r, and $\vec{B}_r$ represent the permeability of free space, recoil permeability, and the remnant flux density of the permanent magnet, respectively. By combining Equations (3) and (4) into (2), we obtain:

$$-\nabla \cdot (\mu_0 \mu_{rec} \nabla V_m - \vec{B}_r) = 0. \tag{5}$$

Equation (5) was used in our numerical COMSOL simulations to describe the material properties of the $Nd_2Fe_{14}B$ block magnets. The μ of polylactic acid (PLA) was also incorporated into the COMSOL simulations to specify the device material.

We used PLA (RepRap Warehouse, Catalog No. R00100002), a thermoplastic polyester with a low melting point, high strength, low thermal expansion, and with a μ comparable to the Petri dishes/culture tubes, provided the necessary durability and versatility to our MF exposure device. The components of the device were 3D printed using PLA filaments with diameters of 1.75 mm with Prusa i3 MK3S and i3 MK3S+ printers.

2.2. Exposure device MF simulations and measurements

COMSOL multiphysics [34] was used to simulate the MFs of the prototype devices to optimize their design before they were 3D printed. The AutoCAD [33] designs of the device were imported into COMSOL and the properties of each material used in the device were defined based on their value of μ (see Table A1).

The $\vec{B}$ in the exposure region of the horizontal MF exposure device was experimentally measured using a Gaussmeter (Alphalab Inc., Model GM2 Gaussmeter), which operates based on the Hall effect [39]. Considering that the two neodymium magnets were kept 132 mm apart from each other in the horizontal and vertical MF exposure devices, the MF generated in both devices are identical. However, depending on the horizontal or vertical configuration of the MF device, the yeast mats grown in Petri dishes experienced different MF strengths. Although the $\vec{B}$ in the exposure region of the assembled horizontal MF configuration was straightforward to measure, the exposure region of the vertical MF device was difficult to access with the Gaussmeter probe when the device was assembled. Therefore, we only measured the $\vec{B}$ for the horizontal configuration of the exposure device. To create this $\vec{B}$ map, a custom cylindrical Gaussmeter probe holder containing 83 equally spaced rectangular holes was designed and 3D printed (Fig. C2A). This permitted us to measure the $\vec{B}$ in each layer at specific positions inside the exposure chamber (Fig. C2B). We were able to limit the $\vec{B}$ mapping to three layers due to the symmetry of the MF. Four $\vec{B}$ readings were obtained for each position in the these layers. The average of these 4 readings was used to obtain the final mapping of $\vec{B}$.

2.3. Yeast MF exposure experiments

Haploid *S. cerevisiae* TBR1 (Σ1278b, matα, *flo11*, tryp) and TBR5 (Σ1278b, matα, *flo11*Δ, tryp) strains were used for the MF exposure experiments [31]. TBR1 (*flo11*) and TBR5 (*flo11*Δ) cells are isogenic apart from the presence or absence of the *flo11* gene, respectively.

Biological replicates of TBR1 and TBR5 were cultured from isogenic colonies in YPD liquid medium at 30 $^{\circ}C$ and shaken overnight on a CO_2-resistant shaker (Thermo Scientific, Catalog no. 88-881-103) at 150 rpm inside an environmental chamber (Thermo Scientific, Catalog no. 13-067-066). yeast extract-peptone-dextrose (YPD) media was made with 5 g of yeast extract (Sigma-Aldrich, Catalog no. Y1625), 10 g of bacto peptone (BD, Catalog no. 211677), 38 mg of adenine (Sigma-Aldrich, Catalogue no. D16), and 7.5 g (or a 1.5 % final concentration) of agar (for agar plates: Fisher Scientific, Catalogue no. BP1423), autoclaved in 450 ml of Type 1 water, and supplemented with glucose (Fisher Scientific,

Catalog no. D16) to a final concentration of 2 %. Liquid TBR1 and TBR5 cultures were inoculated to 5.5×10^5 $cells/ml$ in 5 ml culture tubes (Fisher Scientific, Catalog no. 22-171-606). Agar plates were made by pouring YPD agar medium into a "100 mm" (outer diameter is $\approx$ 92 mm and inner diameter is $\approx$ 88 mm) Petri dish (Fisher Brand, Catalog no. FB0875712) until it was approximately 2/3 full (to minimize agar evaporation and nutrient depletion effects during the experiments). To investigate the effect of MF exposure on spatially-structured yeast populations, YPD agar plates were inoculated with a 2 μl drop of 10^7 $cells/ml$ of either the TBR1 or TBR5 strain in the center of the agar. Six control (no-MF) replicates and six experimental (MF) replicate were used for each experiment; in some experiments, a replicate(s) had to be discarded due to contamination or insufficient agar medium ($N \neq 6$ in these cases).

For the agar culture horizontal and vertical MF exposure experiments, twenty 100 mm Petri dishes (half seeded with TBR1 cells and half seeded with TBR5 cells) were placed inside of four 3D-printed devices. Five TBR1 Petri dishes and five TBR5 Petri dishes were place inside two separate exposure devices (block magnets present), and five TBR1 plates and five TBR5 plates were placed inside two separate control devices (block magnets absent). The MF exposure devices were set up in either the vertical configuration (Fig. 1A) or in the horizontal configuration (Fig. 1B). The horizontal and vertical MFs respectively generate an external magnetic force parallel and perpendicular to the plane of expansion of yeast mats. The experimental and control devices were then placed inside an environmental chamber (Thermo Scientific, Catalog no. 13-067-066) and incubated at 30 $^\circ C$ and 50 % humidity. Yeast mats seeded with TBR1 or TBR5 cells were grown for 25 days. The yeast mats were photographed daily using a Canon EOS Rebel SL3 camera with a Canon EF-S 3 mm f/2.8 Macro IS STM macro lens. The growth rates were evaluated from these photographs as described in Section 2.4.

For the liquid culture horizontal and vertical MF exposure experiments, twenty four 5 ml culture tubes (Fisher Scientific, Catalog no. 22-171-606; half containing TBR1 cells and half containing TBR5 cells) were placed inside four 3D-printed devices. Six TBR1 tubes and six TBR5 tubes were placed inside two separate experimental exposure devices. Another six TBR1 tubes and six TBR5 tubes were places inside two separate control devices. To maintain consistency with the agar culture-MF exposure experiments, the liquid culture-MF exposure experiments were also set up in the horizontal configuration. The experimental and control devices were then placed inside the environmental chamber on the shaker and incubated at 30 $^\circ C$ and 50 % humidity. The liquid TBR1 and TBR5 cultures were grown for 3 days. The growth rates were evaluated and the cultures re-suspended every 12 hours (see Section 2.5).

2.4. Agar culture growth rate measurements

Yeast mat area measurements were obtained daily for 25 days to determine the difference between the mat expansion rate of the control and the MF-exposed TBR1 and TBR5 strains. A quantitative analysis of the mat area expansion rates was performed using the image processing software ImageJ [40]. The resolution of the original images was 6000 by 4000 pixels with an aspect ratio of 3:2. To obtain the area expansion rate from the original images, the original images were cropped to a square ratio (1:1) such that the circumference

of the Petri dish in the image touched each of the four sides of the image. This enabled the accuracy to be maintained when scaling the image pixels by the length of the Petri dish in each image, as the area evaluation of the mats remained consistent throughout the analysis. After extracting the area of the mats from each image, the area expansion rates were obtained by dividing the total area at the end of each day by the number of days. Replicates were quickly removed, imaged, and placed back into the device one at time to minimize interference with the MF exposure; Petri dish lids were left on during imaging to reduce the risk of contamination.

2.5. Liquid culture growth rate measurements

To determine the difference between the growth rates of the control and MF-exposed TBR1 and TBR5 strains in well-mixed YPD liquid cultures, cells were extracted from TBR1-seeded and TBR5-seeded mats using sterile 20 μl pipette tips (Fisher Scientific, Catalog no. 02-707-432). Specifically, twelve cultures of TBR1 cells were extracted from six TBR1 control and six TBR1 MF exposure plates and twelve cultures of TBR5 cells were extracted from six TBR5 control and six TBR5 MF exposure plates and grown in liquid YPD medium for 3 days. Every 12 hours, cell counts were obtained using an automated cell counter (Corning, Catalog no. C-6749) and the cell cultures were re-suspended to an initial concentration of $N_0 = 5.5 \times 10^5$ $cells/ml$ to keep them in log-phase growth. The population growth rate was calculated as follows [41]:

$$r = \frac{1}{t_r} \ln(N(t)/N_0),$$

where t_r is the time interval between re-suspensions and $N(t)$ is the cell count at time t after the re-suspension.

3. Results

3.1. MF Device Optimization and Validation

The MF within the simulated exposure device had a well-defined orientation (Figs. 2A and 3A). Simulations of the vertical configuration of the exposure device produced $\vec{B}$ values ranging from 430 to 730 G along the horizontal surface of the central Petri dish (Fig. 2B). The $\vec{B}$ values ranged from 500 to 1400 G along the central vertical plane of the exposure chamber (Fig. 2C). Simulations of the horizontal configuration of the exposure device produced $\vec{B}$ values ranging from 500 to 1400 G (Fig. 3B,C). In agreement with theory [36], the simulations predicted negligible interference with the MF when the exposure device is fabricated with materials with compatible μ values (Figs. 2A and 3A).

Simulated and experimentally determined $\vec{B}$ maps for the middle layer (layer 3) of the horizontal configuration of the MF exposure device are shown in Figure 4. The simulated $\vec{B}$ values for layer 3 ranged from 514.6 G to 1147.5 G (Figs. 4A and C3A). The experimental $\vec{B}$ values for layer 3 ranged between 550.4 G and 1194.4 G (Figs. 4B and C3B). The simulated and experimental $\vec{B}$ results for layers 1 and 2 are shown in Figures C7 and C8, respectively. On average, each experimental $\vec{B}$ mapping value for layer 3 was 35.5 G different than the corresponding COMSOL simulated value (Fig. C4A). This corresponds to a 4.4 % average

difference between the experimental and simulated $\vec{B}$ values (Fig C4B). Results for layers 1 and 2 follow a similar trend for the differences between the experimental and COMSOL simulated $\vec{B}$ values. For layer 1, each experimental $\vec{B}$ value was 37.2 G less than the corresponding COMSOL simulated value on average, which corresponds to a 5.7 % difference between the experimental and simulated $\vec{B}$ values (Fig. C7). For layer 2, each experimental $\vec{B}$ value was 35.0 G less than the corresponding COMSOL simulated value on average, which corresponds to a 4.5 % difference between the experimental and simulated $\vec{B}$ values (Fig. C8). Overall, the experimental $\vec{B}$ measurements were in good agreement with the simulation results.

3.2. Spatiotemporal yeast mat MF experiments

Horizontal and vertical MF exposure decreased the TBR1 mat area expansion rate (Fig. 5 and Fig. 6, respectively). Statistically significant differences in the average area expansion rate between the experimental (MF exposed) and control (no MF) groups occurred for days 7 to 22 for the horizontal MF exposure experiments (Fig. 5). The average area expansion rate of the TBR1 control group expanded at a linearly increasing rate (Table B1) until saturation around day 18, and then began to decrease. Statistically significant differences in the average area expansion rate between the experimental (MF exposed) and control (no MF) groups occurred for days 6 to 19 and for day 24 for the vertical MF exposure experiments 6. The average area expansion rate of the control group expanded at a linearly increasing rate (Table B2) until saturation around day 15 and then began to decrease. The saturation and subsequent decrease in the average area expansion rates of the faster growing control groups can be attributed to nutrient depletion as the yeast mats expand across the agar surface [29, 42]. The average area expansion rate of the horizontal MF exposed group displayed a slower, monotonic and linearly increasing growth (Table B1). The average area expansion rate of the vertical MF exposed group also displayed a slower, monotonic and linearly increasing growth until saturation around day 17 (Table B2). The average area of the control and horizontal MF exposed TBR1 mats increased exponentially (Table B3). The average area of the control and vertical MF exposed TBR1 mats increased linearly (Table B4).

Horizontal and vertical MF exposure did not impact the TBR5 mat area expansion expansion rate (Fig. 7 and Fig. 8, respectively). Since the TBR5 expansion rate is slower compared to TBR1, the TBR5 average area expansion rates did not saturate during the experiment (Fig. 7 and 8). This likely can be attributed to TBR5 mats not sufficiently depleting the nutrients in the agar media. Experimental and control groups of TBR5 yeast mats displayed a logarithmic average area expansion rates (Table B1), which increased monotonically for the duration of the experiment. The average area of control and MF-exposed TBR5 mats expanded linearly (Table B3).

3.3. Well-mixed planktonic yeast MF experiments

Overall, horizontal and vertical MF exposure did not effect the steady-state growth of TBR1 and TBR5 cells cultured in liquid media (Fig. 9). No significant differences were observed in TBR1 average growth rate between the control and MF-exposed groups at the 12, 36,

48, and 60 hour time points and no significant differences were observed in TBR5 average growth rate between MF exposed and control groups at the 24, 36, 48 and 60 hour time points. Vertical MF exposure did not effect the steady-state growth of TBR1 and TBR5 cells cultured in liquid media (Fig. 10). No significant differences were observed in TBR1 and TBR5 average growth rate between the control and MF-exposed grouops at any time points. The similarity in the growth rates of TBR1 and TBR5 can likely be explained by the negation of the function of the *flo11* gene in liquid media. These results are in agreement with previous TBR1 and TBR5 liquid culture experiments [31, 32].

4. Discussion

In this study, we developed an open-source MF exposure platform to perform magnetobiological experiments on well-mixed and spatially structured populations of microorganisms. Our 3D-printed device was designed in AutoCAD [33] to have interchangeable horizontal and vertical MF configurations and to hold multiple culture tubes and Petri dishes. The strength, size, and position of the magnets were optimized for MF exposure experiments on the budding yeast *Saccharomyces cerevisiae* using numerical simulations in COMSOL [34] together with Gaussmeter measurements. The AutoCAD, COMSOL, and 3D printing files are freely available for use in other MF experiments (see Supporting Materials). In contrast to previous experimental work that focused on individual yeast cells [12], our MF device provides to ability to study the effects of MFs on populations of yeast cells. By using two large Neodymium magnets, the exposure chamber sufficiently large to expose yeast mats/biofilms on agar plates and yeast cells in liquid culture to a homogeneous MF. Additionally, while previous MF exposure experiments were conducted for no longer than 2 days [13, 14, 15, 12], our MF exposure device is able to maintain an uninterrupted MF for longer-term experiments, the importance of which has been previously emphasized [20]. Our compact device can be placed inside of a standard microbiological incubator or environmental chamber to control for confounding environmental variables, such as temperature, that affect growth and gene expression in yeast [43]. We note that our MF device can be used to explore MF effects on a microorganisms beyond yeast, for instance, planktonic bacteria and bacterial biofilms.

We used our MF exposure device to investigate the effects of MFs on the growth of two genetically engineered *S. cerevisiae* strains in both agar and liquid media. We discovered that horizontal and vertical MFs slowed the spatially-structured expansion of TBR1 yeast mats on agar, but that MFs did not affect the expansion of TBR5 yeast mats. We also found that vertical and horizontal MFs did not affect the growth of well-mixed TBR1 and TBR5 yeast cells in liquid media. We hypothesize that the decreased expansion rate of horizontal MF-exposed TBR1 yeast mats results from spatial hindrance in the 2D expansion of this strain [31] combined with the magnetic properties of microtubules [12, 44, 45]. As the mitotic spindle is composed of [46] and oriented [47] by microtubules, the presence of a horizontal MF may cause the budding yeast cells to align their long axis along the direction of the MF [20, 12]. Partial or complete alignment of cells to the MF at the expanding boundary of a yeast mat may introduce competition among cells attempting to bud into unoccupied space on the agar surface. These experimental results qualitatively

agree with computational predictions [20]. Related demography-dispersal trade-offs effects have recently been reported in competing and evolving TBR1 and TBR5 yeast mats in the absence of MFs [48]. As for vertical MF exposure, we hypothesize that the magnetic force negates the surface adhesion of *Flo11*, which allows TBR1 to expand in 3D (similar to TBR5), leading to slower radial expansion across the agar surface. MF-induced steric hindrance may also explain the previously observed slowed growth of phytopathogenic fungi exposed to MFs [17]; increased cell-to-cell contact forces resulting from MF alignment may destabilize polarized growth machinery [49]. While TBR5 cells would experience similar MF orientation effects as TBR1 cells, the fact that TBR5 mats expand in 3D across the agar surface may reduce spatial hindrance effects at the expanding mat front. No MF-related effects were observed when planktonic TBR1 and TBR5 strains were grown in liquid media. This can likely be attributed to negation of *flo11* in well-mixed environments, rendering the fitness of planktonic TBR1 and TBR5 cells equal.

Previous studies have highlighted the importance of studying the non-linear effects of MF on biological systems at specific flux densities (e.g., [6]). As our device was design to expose microbial populations to a range of flux density values, the current design lacks the ability to generate a single MF strength through out the exposure region. Although we simulated and experimentally mapped the flux density values at various locations within the exposure region, we did not evaluate the biological effects of MFs at specific flux density values. Such studies may be performed by adapting our MF exposure platform to incorporate a Gaussmeter probe and multiple cameras or a stage-mounted camera. We also note that studying the effects of inhomogeneous MFs on microbial populations may prove to be a promising line of future research. To facilitate this research, smaller magnets could be used with our device to expose microbiological samples to MF edge effects. MF effects at the single cell-level [12] may be important for to elucidate the mechanisms underlying our population-scale experimental results. Our MF device could be augmented with a camera for microscopic imaging to study MF effects in real-time at the single-cell level in microbial populations. Other future improvements to our MF device include using a 3D printed material other than PLA (which has rigidity at temperatures between 45 °C and 60 °C [50]), such as nylon of carbon fiber that can withstand the high temperature and pressure of an autoclave [51]. Finally, performing experiments with many exposure devices in parallel will ensure sufficient biological replicates with identical vertical MF conditions.

It will be imperative to elucidate the biophysical mechanisms underlying our experimental results. The magnetization of microtubules should be investigated in the context of yeast mat and biofilm development. Previous studies have reported magnetic properties of microtubules [45, 52] and it has been proposed that the polarization of microtubules is responsible for the alignment of *S. cerevisiae* with MFs [12]. As radical pairs may play a role in microtubule reorganization, this should also be investigated as possible mechanism underlying magnetic phenomena in yeast [53]. Overall, we anticipate that our MF exposure device and experimental findings will advance our fundamental understanding of magnetic phenomena in microbes.

Supporting Materials

Supporting materials include ten figures, five tables, and ten supplemental figures.

Experimental data available at: `https://data.mendeley.com/datasets/ycm2rgcfdx/4`.

Exposure device design DIY is available at: `https://github.com/CharleboisLab/Exposure-Design-DIY---AutoCAD-and-STL-Files.git`.

Acknowledgments

The authors thank Prof. Mark Freeman for guidance on 3D printing and for access to a Gaussmeter and Prof. Jack Tuszynski for helpful discussions.

DC was supported by funding from the Government of Canada's NSERC Discovery Grant (RGPIN-2020-04007) and Launch Supplement (DGECR-2020-00197). EL was supported by the University of Alberta's URI Undergraduate Researcher Stipend. This work was completed in part with resources provided by The Shack at the University of Alberta to 3D print prototypes of the magnetic field device.

Finally, we thank the two anonymous reviewers for their helpful comments on the manuscript.

Author contributions

DC conceptualised the study. AB designed, modeled, built, and validated the magnetic field device. AB performed the yeast experiments with assistance from EL. AB visualised and analysed the results. DC and AB wrote the manuscript. DC supervised the study.

Declaration of Interests

The authors declare no competing interests.

5. Figures

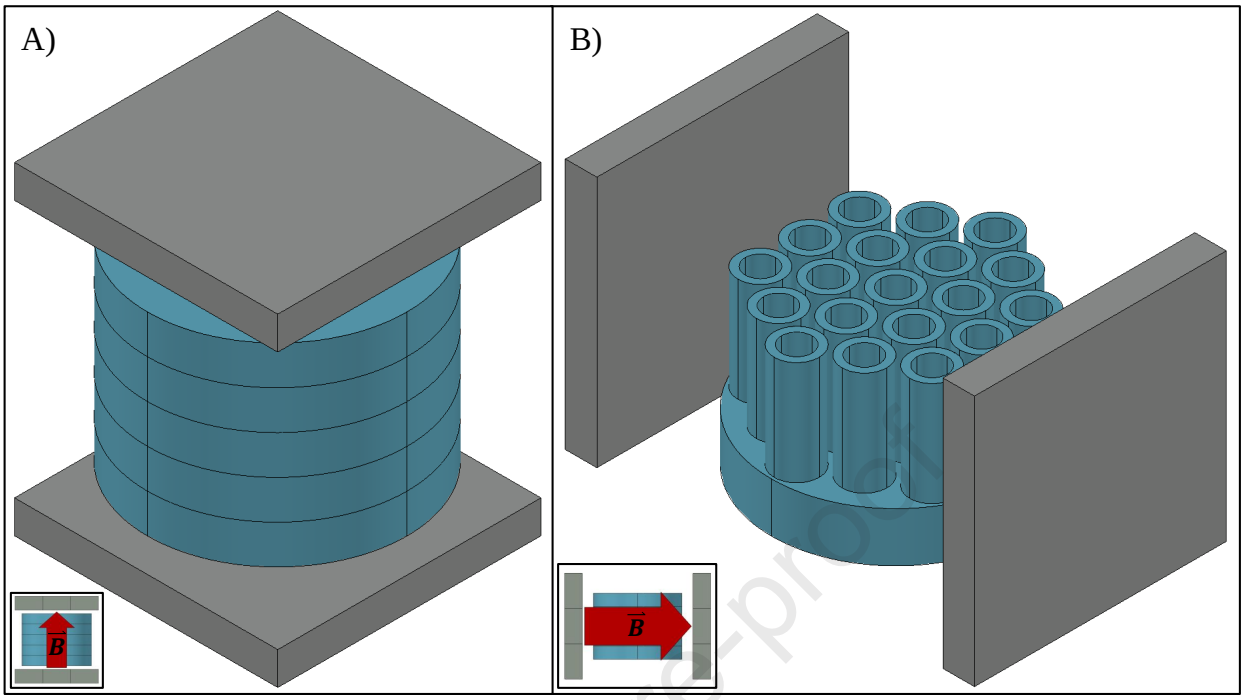

Figure 1: AutoCAD [33] schematics showing some different configurations of the magnetic field device. (A) Schematic of the vertical configuration of the device, which was used to expose yeast grown on semi-solid media in Petri dishes to a static vertical magnetic field (MF). Petri dishes are shown in blue. (B) Schematic of the horizontal configuration of the device, which was used to expose yeast grown in liquid media in cell culture tubes to a static horizontal MF. Culture tubes and holder are shown in blue. The grey blocks in (A) and (B) represent the Neodymium magnets; insets show the direction of the magnetic flux density ($\vec{B}$).

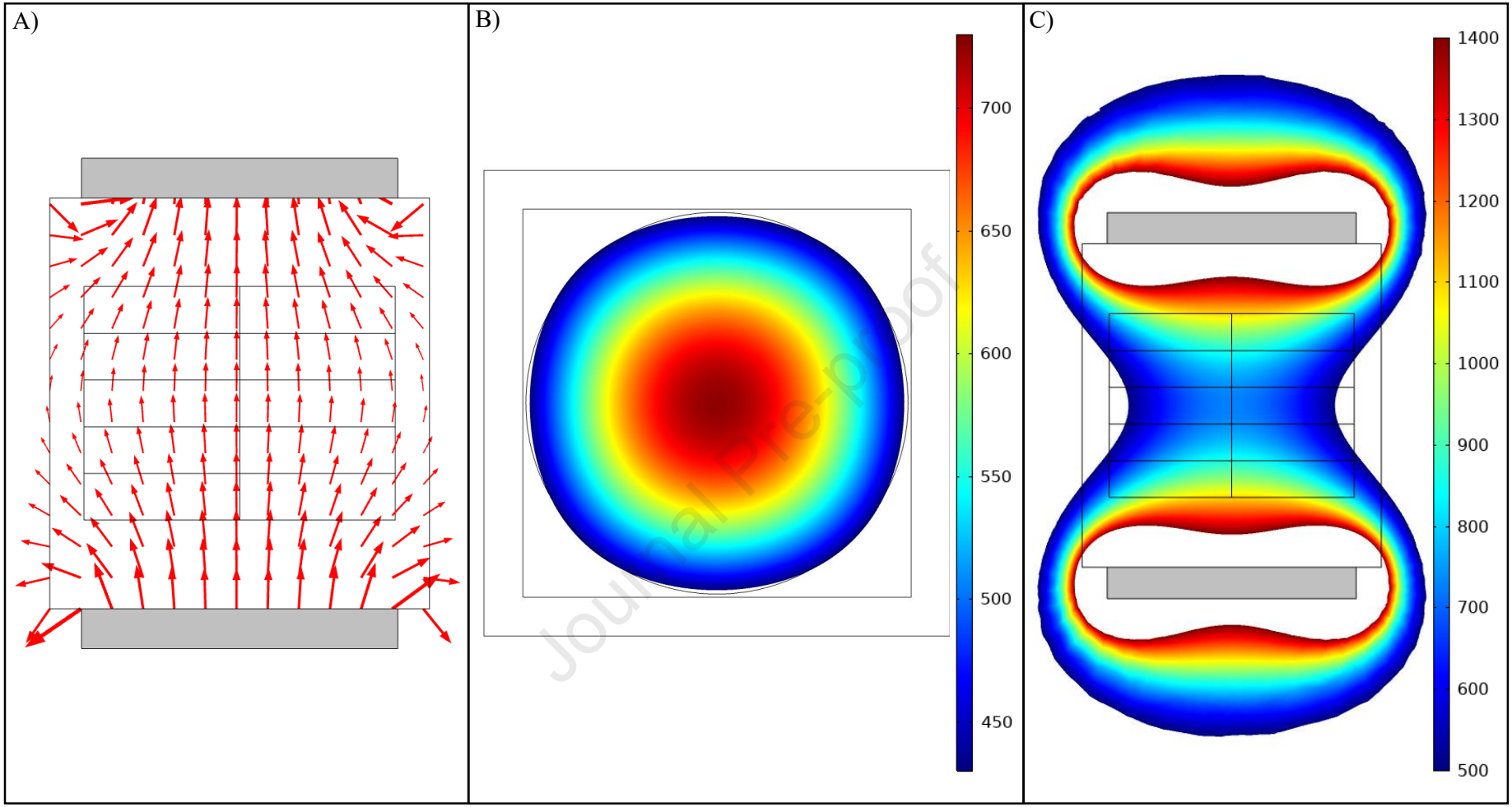

Figure 2: Simulation of the vertical configuration of the magnetic field device. (A) COMSOL [34] simulation of the directional orientation of the magnetic field. (B) COMSOL simulation of the magnetic flux density ($\vec{B}$) along the central horizontal plane of the exposure device. The point of view of this panel is from above looking down at the central Petri dish. (C) COMSOL simulation of the $\vec{B}$ along the central vertical plane of the exposure device. The point of view of this panel is from the side of the exposure device looking at the sides of the Petri dishes. The grey blocks in (A) and (C) denote the Neodymium magnets. The colorbars denote $\vec{B}$ in Gauss (G).

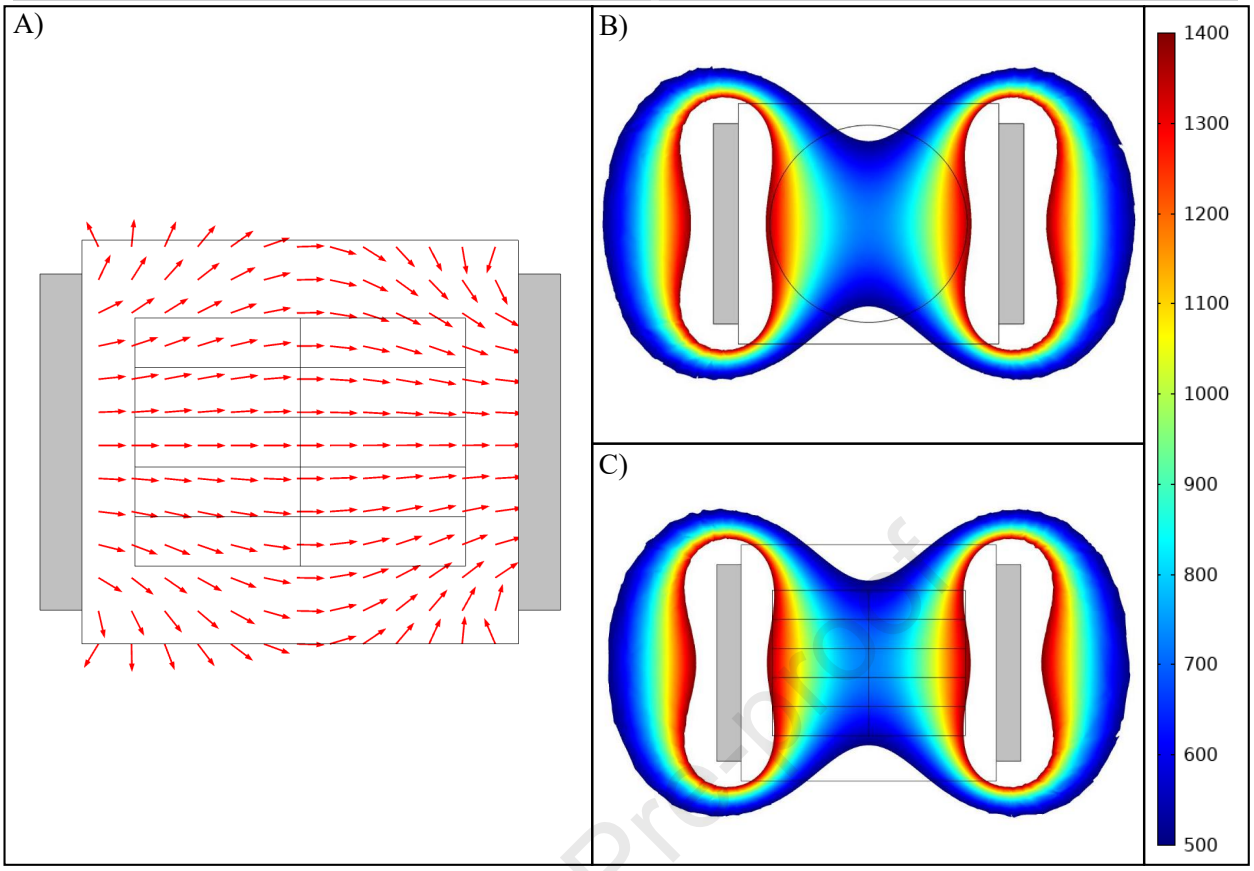

Figure 3: Simulation of the horizontal configuration of the magnetic field device. (A) COMSOL [34] simulation results of the directional orientation of the magnetic field. (B) COMSOL simulation of the magnetic flux density ($\vec{B}$) along the central horizontal plane of the exposure device. The point of view of this panel is from above looking down at the central Petri dish. (C) COMSOL simulation of the $\vec{B}$ along the central plane from the side view of the exposure device. The grey blocks in (A)-(C) represent the Neodymium magnets. The colorbar denotes $\vec{B}$ in Gauss (G).

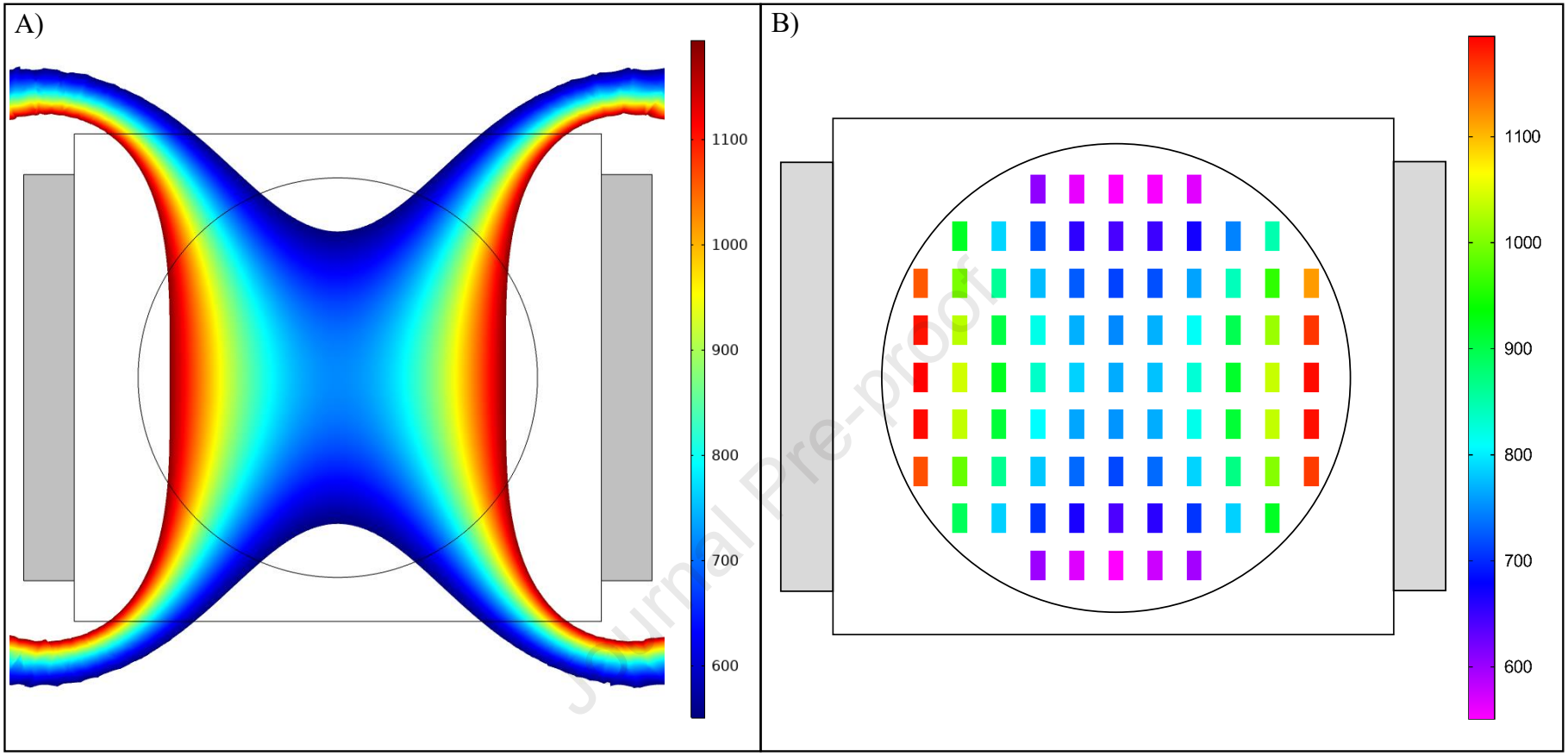

Figure 4: Comparison of simulation and experimental measurements of the horizontal configuration of the magnetic field device. (A) Top view of a COMSOL [34] simulation of the magnetic flux density ($\vec{B}$) along the middle layer (layer 3) of the exposure chamber of the device. (B) Top view of the experimental $\vec{B}$ mapping of the sample exposure region of the device corresponding to (A). The grey blocks in (A) and (B) represent the Neodymium magnets. The colorbars denotes $\vec{B}$ in Gauss (G).

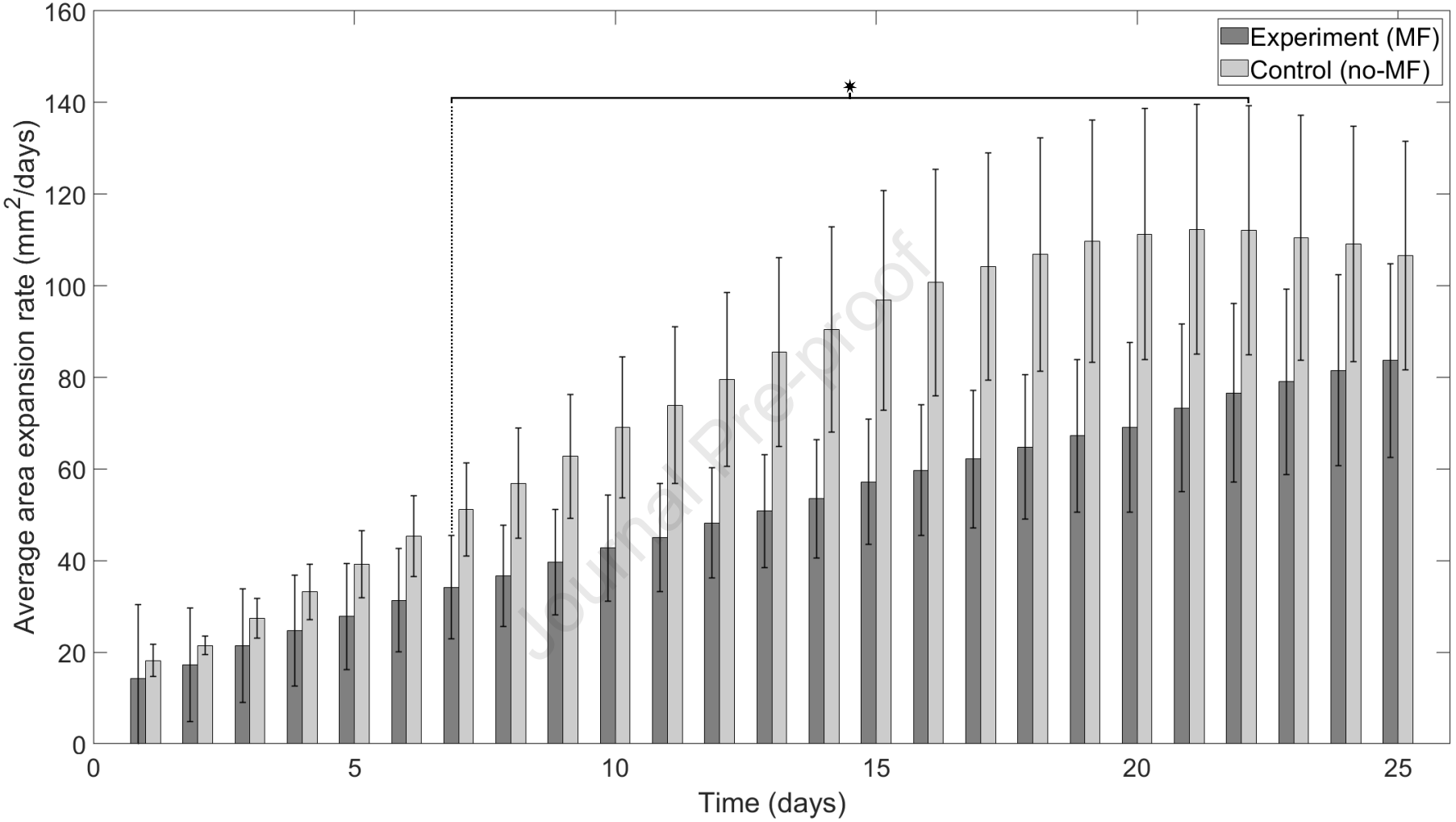

Figure 5: Average area expansion rates of TBR1 yeast mats in agar plates in the presence and absence of a horizontal magnetic field (MF). TBR1-seeded control (no-MF) and experimental (MF) mats grown on agar. An independent samples t-test was performed to compare the average expansion rates for a sample size of $N = 5$. A significant difference in average area expansion rates independent samples t-test ($p < 0.05$, denoted by an asterisk) was found for days 7 to 22. Error bars denote standard deviation.

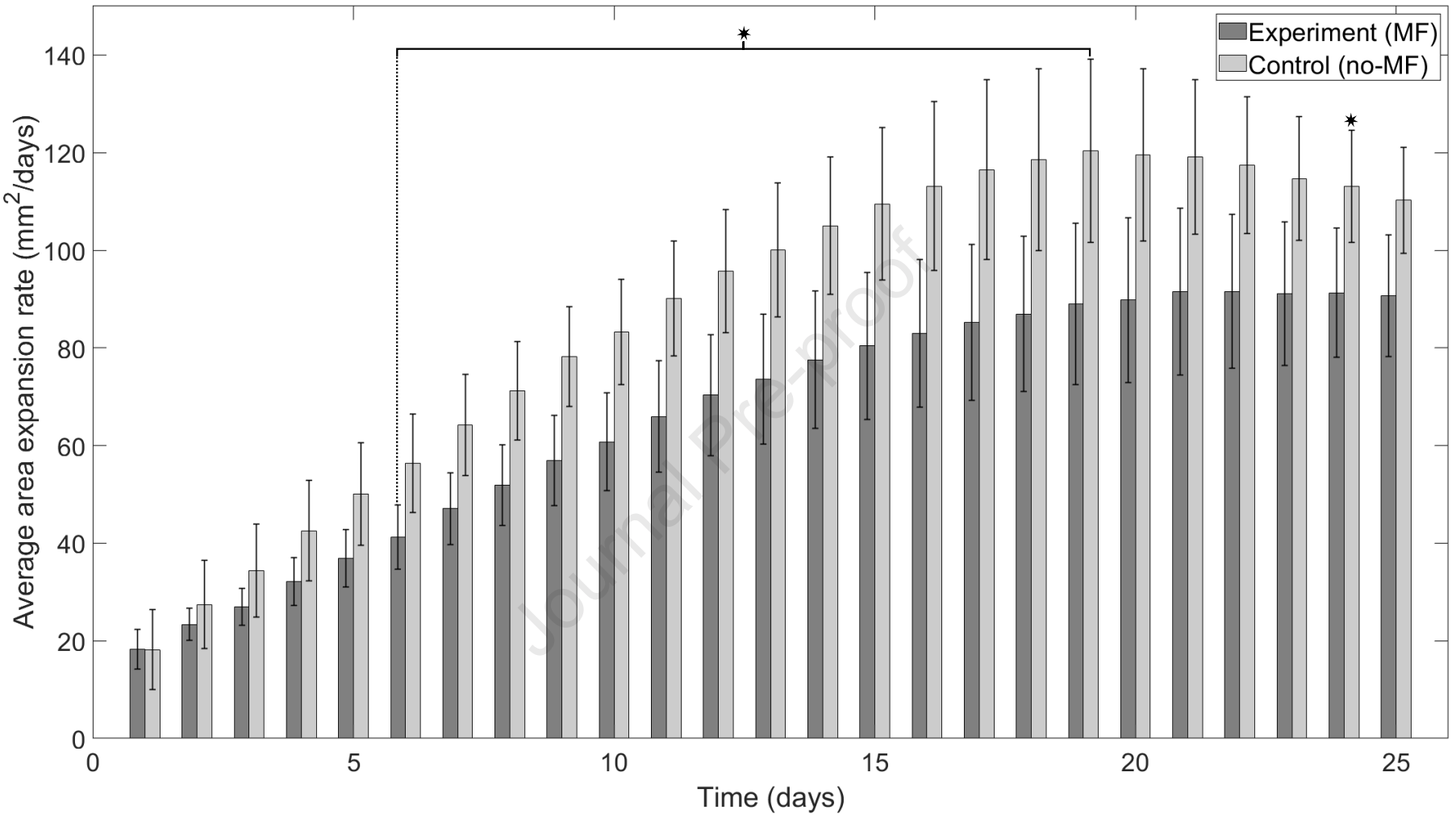

Figure 6: Average area expansion rates of TBR1 yeast mats in agar plates in the presence and absence of a vertical magnetic field (MF). TBR1-seeded control (no-MF) and experimental (MF) mats grown on agar. An independent samples t-test was performed to compare the average expansion rates for a sample size of $N = 4$. A significant difference in average area expansion rates independent samples t-test ($p < 0.05$, denoted by an asterisk) was found for days 6 to 19 and on day 24. Error bars denote standard deviation.

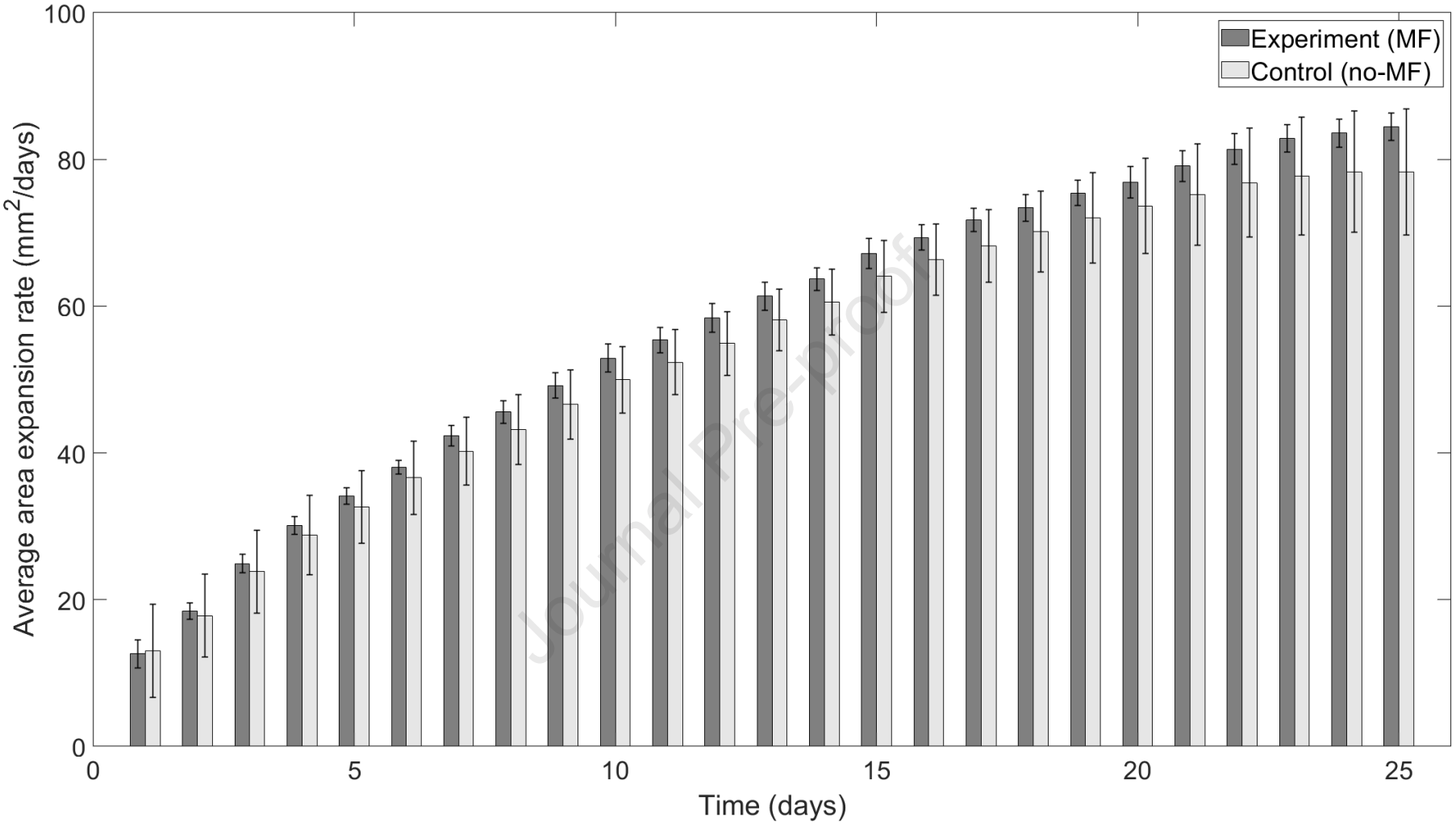

Figure 7: Average area expansion rates of TBR5 yeast mats in the presence and absence of a horizontal magnetic field (MF). TBR5-seeded control (no-MF) and experimental (MF) mats grown on agar plates. An independent samples t-test was performed to compare the average expansion rates for a sample size of $N = 3$. No significant difference in average area expansion rates ($p > 0.05$) was found for any day. Error bars denote standard deviation.

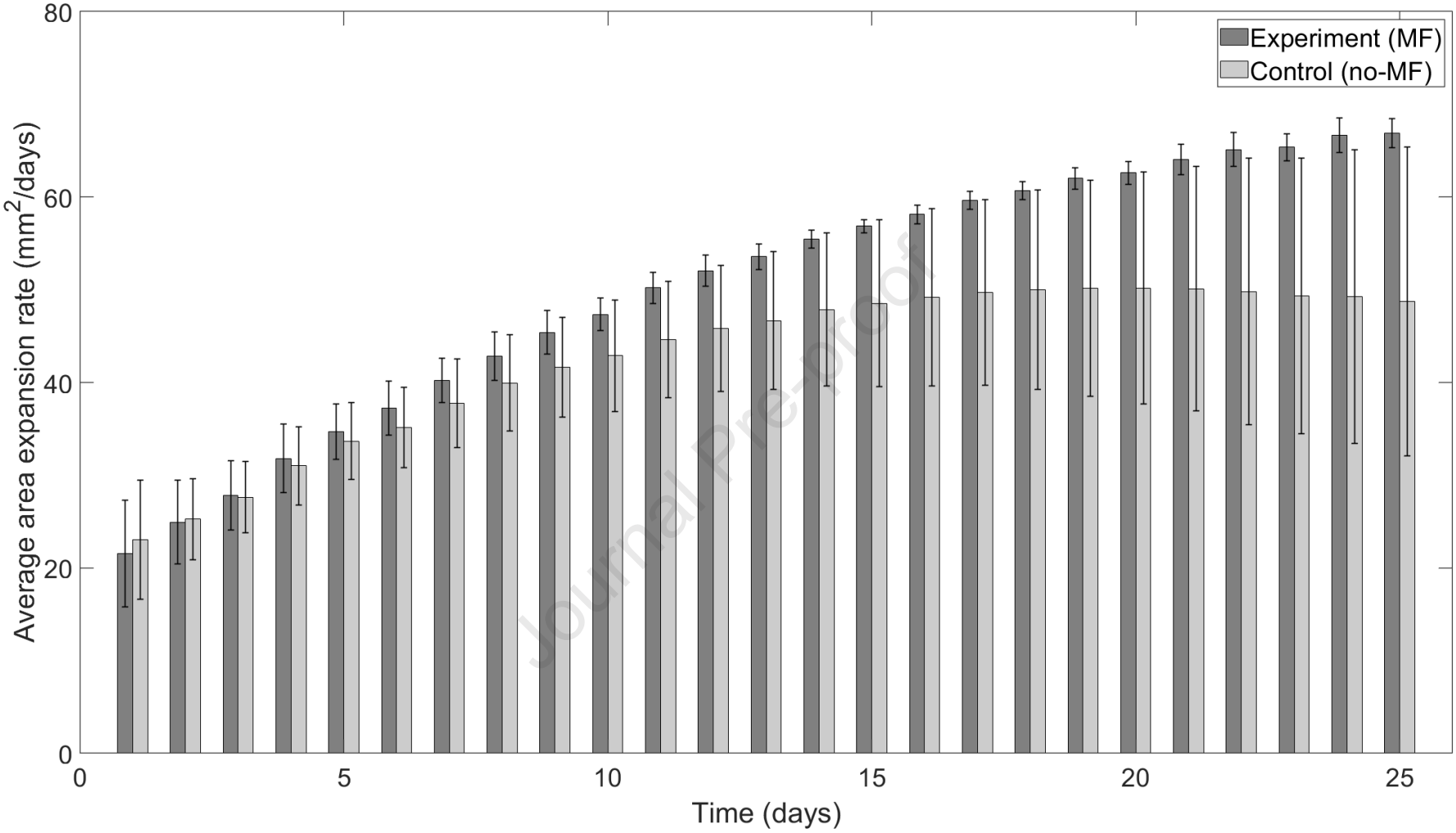

Figure 8: Average area expansion rates of TBR5 yeast mats in the presence and absence of a vertical magnetic field (MF). TBR5-seeded control (no-MF) and experimental (MF) mats grown on agar plates. An independent samples t-test was performed to compare the average expansion rates for a sample size of $N = 4$. No significant difference in average area expansion rates ($p > 0.05$) was found for any day. Error bars denote standard deviation.

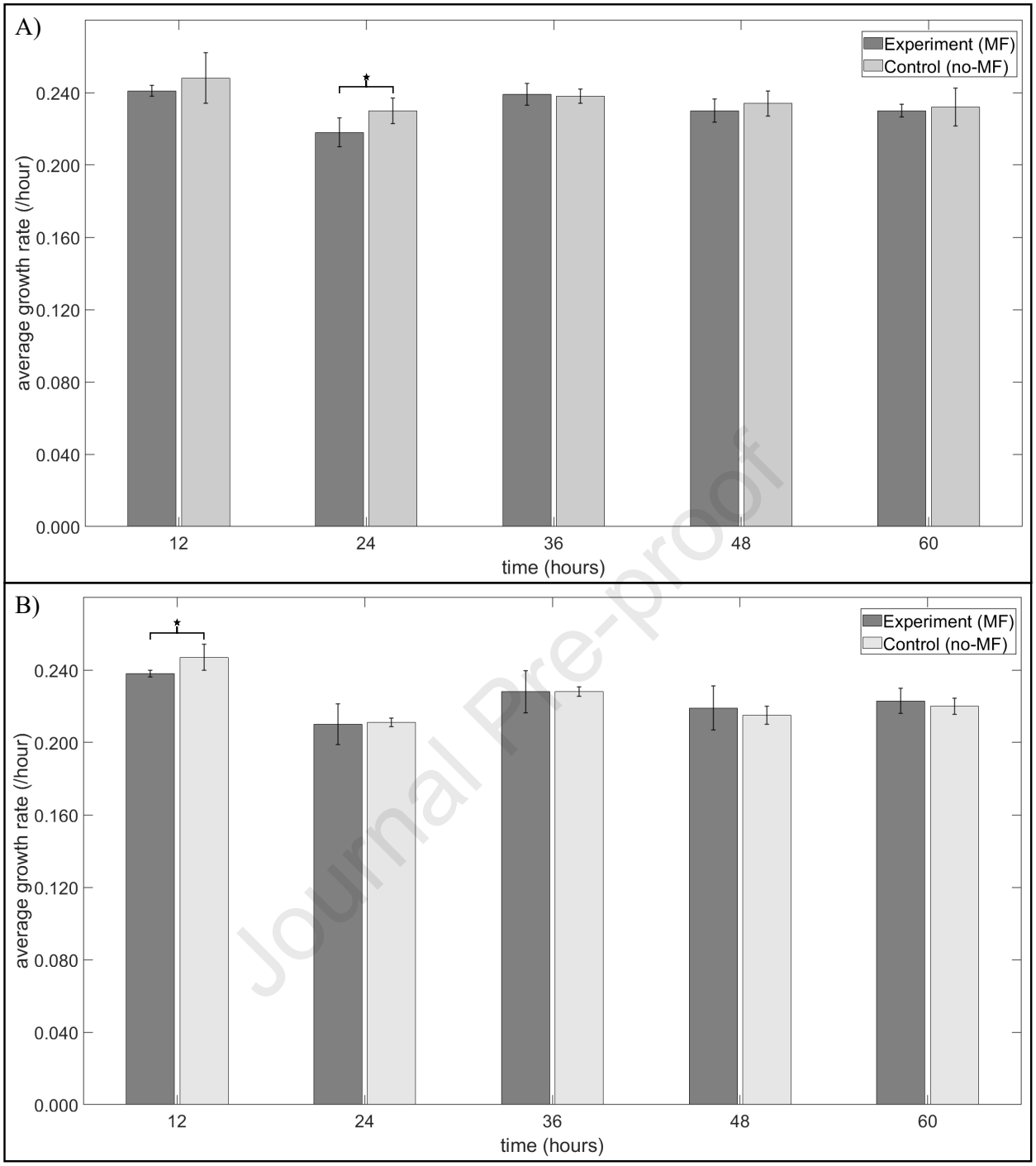

Figure 9: Average growth rates of TBR1 and TBR5 cells in liquid culture in the presence and absence of a horizontal magnetic field (MF). (A) Average growth rates of TBR1. An independent samples t-test was performed to compare the average growth rates between the exposure (MF) and control (no-MF) replicates for a sample size of $N = 6$. A significant difference ($p < 0.05$) was only observed at the 24 hour time point. (B) Average growth rate of TBR5. An independent samples t-test was performed to compare the average growth rates between the exposure (MF) and control (no-MF) replicates for a sample size of $N = 6$. A significant difference ($p < 0.05$) was only observed at the 12 hour time point. Error bars denote standard deviation.

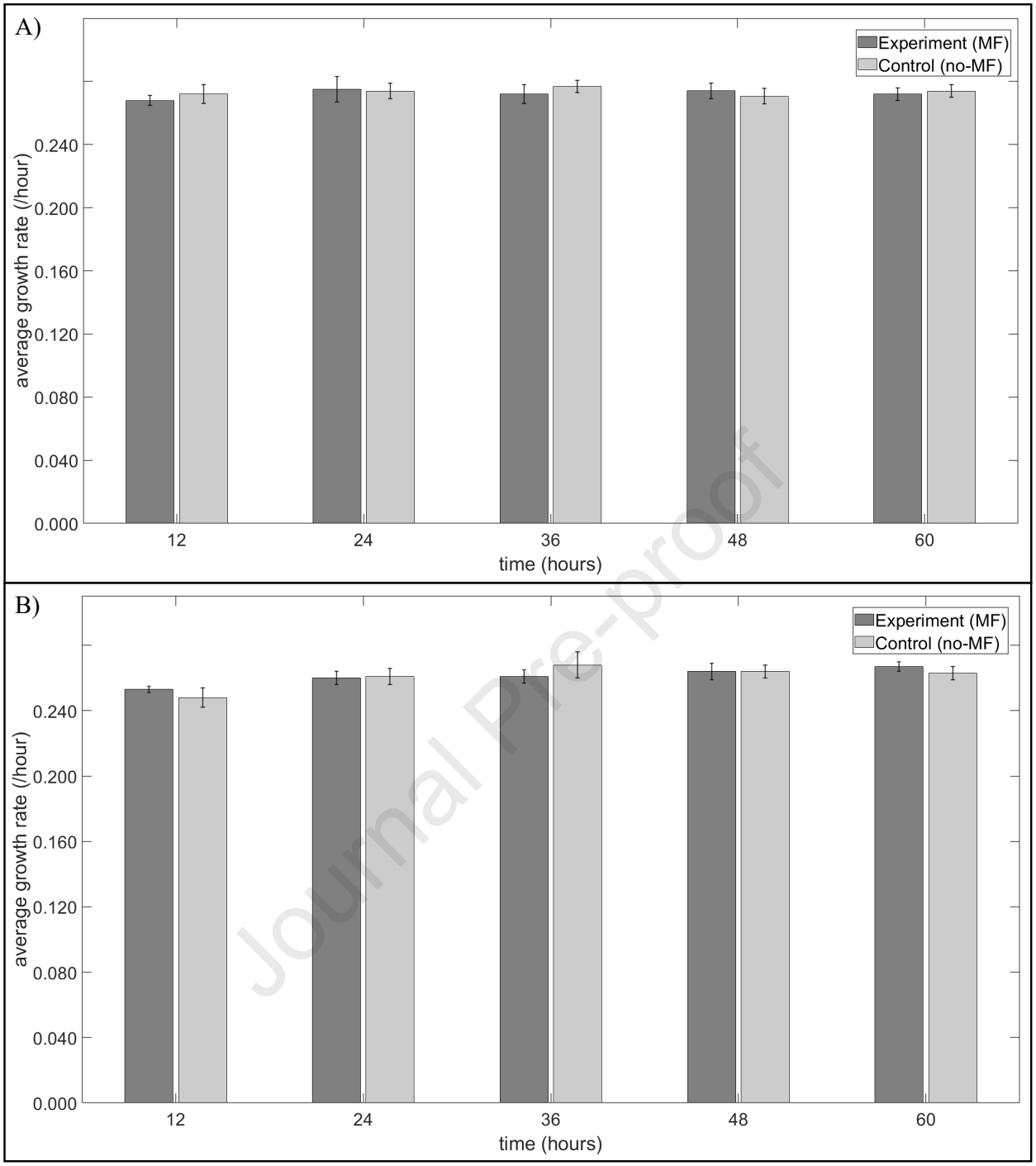

Figure 10: Average growth rates of TBR1 and TBR5 cells in liquid culture in the presence and absence of a vertical magnetic field (MF). (A) Average growth rates of TBR1. (B) Average growth rates of TBR5. For (A) and (B), an independent samples t-test was performed to compare the average growth rates between the exposure (MF) and control (no-MF) replicates for a sample size of $N = 6$; no significant difference ($p > 0.05$) was observed at any time point. Error bars denote standard deviation.

References

[1] W. Erdmann, H. Kamita, J. Z. Kosicki, and L. Kaczmarek. How the geomagnetic field influences life on earth - an integrated approach to geomagnetobiology. *Origins of Life and Evolution of Biospheres*, 51:231–257, 2021.

[2] S. Johnsen and K. J. Lohmann. Magnetoreception in animals. *Physics Today*, 61:29–35, 2008.

[3] N. Hirota, J. Nakagawa, and K. Kitazawa. Effects of a magnetic field on the germination of plants. *Journal of Applied Physics*, 85:5717–5719, 1999.

[4] T. Higashi, N. Ashida, and T. Takeuchi. Orientation of blood cells in static magnetic field. *Physica B*, 237-238:616–620, 1997.

[5] T. Higashi, A. Yamagishi, T. Takeuchi, N. Kawaguchi, S. Sagawa, S. Onishi, and M. Date. Orientation of erythrocytes cells in a strong static magnetic field. *Blood*, 82:1328–1334, 1993.

[6] A. V. Van Huizen, J. M. Morton, L. J. Kinsey, D. G. Von Kannon, M. A. Saad, T. R. Birkholz, J. M. Czajka, J. Cyrus, F. S. Barnes, and W. S. Beane. Weak magnetic fields alter stem cell–mediated growth. *Science Advances*, 5:eaau7201, 2019.

[7] G. Vargas, J. Cypriano, T. Correa, P. Leão, D. A. Bazylinski, and F. Abreu. Applications of magnetotactic bacteria, magnetosomes and magnetosome crystals in biotechnology and nanotechnology: Mini-review. *Molecules*, 23:2438, 2018.

[8] A. Jóskowiak, C. L. Nogueira, S. P. Costa, A. P. Cunha, P. P. Freitas, and C. M. Carvalho. A magnetic nanoparticle-based microfluidic device fabricated using a 3d-printed mould for separation of *Escherichia coli* from blood. *Microchimica Acta*, 190:356, 2023.

[9] S. Pacios-Michelena, R. Rodríguez-Herera, G. Rincón-Enríquez, R. Ramos-Gonzáles, A. C. Flores-Gallegos, M. L. Chávez-Gonzáles, E. P. Segura-Ceniceros, and A. Ilyina. *Escherichia coli* **DH5**α functionalised magnetite nanoparticles applied for the magnetic extraction of bacteriophages. *Micro Nano Letters*, 15:1134–1139, 2020.

[10] T. Saliev, D. Begimbetova, A. R. Masoud, and B. Matkarimov. Biological effects of non-ionizing electromagnetic fields: Two sides of a coin. *Progress in Biophysics and Molecular Biology*, 141:25–36, 2019.

[11] D. Botstein and R. Fink. Yeast: An experimental organism for 21st century biology. *Genetics*, 189:695–704, 2011.

[12] S. Egami, Y. Naruse, and H. Watarai. Effect of static magnetic fields on the budding of yeast cells. *Bioelectromagnetics*, 31:622–629, 2010.

[13] D. M. Binninger and V. Ungvichian. Effects of 60 hz ac magnetic fields on gene expression following exposure over multiple cell generations using Saccharomyces cerevisiae. *Bioelectrochemistry and Bioenergetics*, 43:83–89, 1997.

[14] M. Ikehata, M. Iwasakaand J. Miyakoshi, S. Ueno, and T. Koana. Effects of intense magnetic fields on sedimentation pattern and gene expression profile in budding yeast. *Journal of Applied Physics*, 93:6724–6726, 2003.

[15] M. Iwasaka, M. Ikehata, J. Miyakoshi, and S. Ueno. Strong static magnetic field effects on yeast proliferation and distribution. *Bioelectrochemistry*, 65:59–68, 2004.

[16] M. J. Ruiz-Gomez, M. I. Prieto-Barcia, E Ristori-Bogajo, and M Martínez-Morillo. Static and 50 hz magnetic fields of 0.35 and 2.45 mt have no effect on the growth of *Saccharomyces cerevisiae*. *Bioelectrochemistry*, 64:151–155, 2004.

[17] P. Nagy and G. Fischl. Effect of static magnetic field on growth and sporulation of some plant pathogenic fungi. *Bioelectromagnetics*, 25:316–318, 2004.

[18] R. Ruzic, N. Gogala, and I. Jerman. Sinusoidal magnetic fields: Effects on the growth and ergosterol content in mycorrhizal fungi. *Electro- and Magnetobiology*, 16:129–142, 1997.

[19] J. Novak, L. Strasak, L. Fojt, I. Slaninova, and V. Vetterl. Effects of low-frequency magnetic fields on the viability of yeast Saccharomyces cerevisiae. *Bioelectrochemistry*, 70:115–121, 2007.

[20] R. Hall and Daniel A. Charlebois. Lattice-based monte carlo simulation of the effects of nutrient concentration and magnetic field exposure on yeast colony growth and morphology. *In Silico Biology*, 14:53–69, 2021.

[21] D.B. Lyle, X. H. Wang, R. D. Ayotte, A. R. Sheppard, and W. R. Adey. Calcium uptake by leukemic and normal t-lymphocytes exposed to low frequency magnetic fields. *Bioelectromagnetics*, 12:145–156,

1991.

[22] D. Broers, G. Kraeplin, I. Lamprecht, and O. Schultz. *Mycotypha africana* in low-level athermic elf magnetic fields. *Bioelectrochemistry and Bioenergetics*, 16:281–291, 1992.

[23] R. J. Reiter and B. A. Richardson. Magnetic field effects on pineal indoleamine metabolism and possible biological consequences. *The FASEB Journal*, 6:2283–2287, 1992.

[24] H. Desjobert, J. Hillon, M. Adolphe, G. Averlant, and J. Nafziger. Effects of 50 hz magnetic fields on c-myc transcript levels in nonsynchronized and synchronized human cells. *Bioelectromagnetics*, 16:277–283, 1995.

[25] V. P. P. Alonso, J. G. Lemos, and M. D. do Nascimento. Yeast biofilms on abiotic surfaces: Adhesion factors and control methods. *International Journal of Food Microbiology*, 400:110265, 2023.

[26] W. S. Lo and A. M. Dranginis. The cell surface flocculin flo11 is required for pseudohyphae formation and invasion by *Saccharomyces cerevisiae*. *Molecular Biology of the Cell*, 9:161–171, 1998.

[27] B. Guo, C. A. Styles, Q. Feng, and G. R. Fink. A *Saccharomyces* gene family involved in invasive growth, cell-cell adhesion, and mating. *Proceedings of the National Academy of Sciences of the United States of America*, 97:12158–12163, 2000.

[28] T. B. Reynolds and G. R. Fink. Bakers' yeast, a model for fungal biofilm formation. *Science*, 291:878–881, 2001.

[29] T. B. Reynolds, A. Jansen, X. Peng, and G. R. Fink. Mat formation in *Saccharomyces cerevisiae* requires nutrient and ph gradients. *Eukaryotic Cell*, 7:122–130, 2008.

[30] T. B. Reynolds. Going with the flo: The role of flo11-dependent and independent interactions in yeast mat formation. *Journal of Fungi*, 4:132, 2018.

[31] L. Chen, J. Noorbakhsh, R. M. Adams, J. Samaniego-Evans, G. Agollah, D. Nevozhay, J. Kuzdzal-Fick, P. Mehta, and G. Balázsi. Two-dimensionality of yeast colony expansion accompanied by pattern formation. *PLOS Computational Biology*, 10:e1003979, 2014.

[32] B. Purevdorj-Gage, M. E. Orr, P. Stoodley, K. B. Sheehan, and L. E. Hyman. The role of flo11 in Saccharomyces cerevisiae biofilm development in a laboratory based flow-cell system. *FEMS Yeast Research*, 7:372–379, 2007.

[33] 2021 Autodesk Inc. AutoCAD 2022. `https://manage.autodesk.com/products`, Version - S.51.0.0 AutoCAD 2022.

[34] COMSOL Inc. COMSOL Multiphysics. `https://www.comsol.com/comsol-multiphysics`, Version - 6.0.

[35] H. Zadeh-Haghighi and C. Simon. Magnetic field effects in biology from the perspective of the radical pair mechanism. *Journal of the Royal Society Interface*, 19:20220325, 2022.

[36] O. Heaviside. *Electrical Papers. Vol 2.* Macmillan and Co, 1894.

[37] COMSOL Inc. Finite Element Analysis (FEA) Software `https://www.comsol.com/multiphysics/fea-software?parent=finite-element-method-042-62-22` Last modified: 2017-02-21, Accessed on: 2023-11-17.

[38] J. D. Jackson. *Classical Electrodynamics - 3rd Edition.* John Wiley Sons, 1998.

[39] E. H. Hall. On a new action of the magnet on electric currents. *American Journal of Mathematics*, 2:287–292, 1879.

[40] W. S. Rasband. ImageJ. U.S National Institute of Health, Bethesda, Maryland, USA, `https://imagej.net/ij/index.html`, 1997-2018, Version - 1.53k.

[41] D. A. Charlebois and G. Balázsi. Modeling cell population dynamics. *In Silico Biology*, 13:21–39, 2019.

[42] Amy L. Forehand, Dulgunn Myagmarsuren, Ziyan Y. Chen, and Helen. A. Murphy. Variation in ph gradients and flo11 expression in mat biofilms from environmental isolates of the yeast *Saccharomyces cerevisiae*. *MicrobiologyOpen*, 11:e1277, 2022.

[43] Daniel A. Charlebois, K. Hauser, S. Marshall, and G. Balázsi. Multiscale effects of heating and cooling on genes and gene networks. *PNAS*, 115:E10797–E10806, 2018.

[44] R. Emura, T. Takeuchi, Y. Nakaoka, and T. Higashi. Analysis of anisotropic diamagnetic susceptibility of a bull sperm. *Bioelectromagnetics*, 24:347–355, 2003.

[45] T. Takeuchi, Y. Nakaoka, R. Emura, and T. Higashi. Diamagnetic orientation of bull sperms and related materials in static magnetic fields. *Journal of the Physical Socienty of Japan*, 71:363–368, 2002.

[46] H. V. Goodson and E. M. Jonasson. Microtubules and microtubule-associated proteins. *Cold Spring Harbor Perspectives in Biology*, 10:a022608, 2018.

[47] J. L. Carminati and T. Stearns. Microtubules orient the mitotic spindle in yeast through dynein-dependent interactions with the cell cortex. *Journal of Cell Biology*, 138:629–641, 1997.

[48] R. Hall, A. Bandara, and Daniel A. Charlebois. Fitness effects of a demography-dispersal trade-off in expanding *Sacchcaromyces cerevisiae* mats. *Physical Biology*, 21:026001, 2024.

[49] R. Mishra, N. Minc, and M. Peter. Cells under pressure: how yeast cells respond to mechanical forces. *Trends in Microbiology*, 30:495–510, 2022.

[50] S. Farah, D. G. Anderson, and R. Langer. Physical and mechanical properties of pla, and their functions in widespread applications — a comprehensive review. *Advanced Drug Delivery Reviews*, 107:367–392, 2016.

[51] V. R. Sastri. *Plastics in Medical Devices (Third Editon)*, chapter 4, pages 68–71. William Andrew Publishing, 2022.

[52] L. Zhang, Y. B. Hou, Z. Y. Li, X. M. Ji, Z. Wang, H. Z. Wang, X. F. Tian, F. Z. Yu, Z. Y. Yang, L. Pi, T. J. Mitchson, Q. Y. Lu, and X. Zhang. 27 ultra-high static magnetic field changes orientation and morphology of mitotic spindles in human cells. *eLife*, 6:e22911, 2017.

[53] H. Zadeh-Haghighi and C. Simon. Radical pairs may play a role in microtubule reorganization. *Scientific Reports*, 12:6109, 2022.